JACS
JOURNAL OF THE AMERICAN CHEMICAL SOCIETY
Article
pubs.acs.org/JACS

# Functional Near Infrared-Emitting $Cr^{3+}/Pr^{3+}$ Co-Doped Zinc Gallogermanate Persistent Luminescent Nanoparticles with Superlong Afterglow for *in Vivo* Targeted Bioimaging

Abdukader Abdukayum,[†,§] Jia-Tong Chen,[‡] Qiang Zhao,[‡] and Xiu-Ping Yan*[,†]

[†]State Key Laboratory of Medicinal Chemical Biology (Nankai University), Synergetic Innovation Center of Chemical Science and Engineering (Tianjin), and Research Center for Analytical Sciences, College of Chemistry, and [‡]College of Life Sciences, Nankai University, 94 Weijin Road, Tianjin 300071, China

Supporting Information

**ABSTRACT:** Near infrared (NIR)-emitting persistent luminescent nanoparticles (PLNPs) have great potential for *in vivo* bioimaging with the advantages of no need for *in situ* excitation, high signal-to-noise ratio, and deep tissue penetration. However, functional NIR-emitting PLNPs with long afterglow for long-term *in vivo* imaging are lacking. Here, we show the synthesis of NIR-emitting long-persistent luminescent nanoparticles (LPLNPs) $Zn_{2.94}Ga_{1.96}Ge_2O_{10}:Cr^{3+},Pr^{3+}$ by a citrate sol–gel method in combination with a subsequent reducing atmosphere-free calcination. The persistent luminescence of the LPLNPs is significantly improved via codoping $Pr^{3+}/Cr^{3+}$ and creating suitable Zn deficiency in zinc gallogermanate. The LPLNP powder exhibits bright NIR luminescence in the biological transparency window with a superlong afterglow time of over 15 days. A persistent energy transfer between host and $Cr^{3+}$ ion in the LPLNPs is observed and its mechanism is discussed. PEGylation greatly improves the biocompatibility and water solubility of the LPLNPs. Further bioconjugation with c(RGDyK) peptide makes the LPLNPs promising for long-term *in vivo* targeted tumor imaging with low toxicity.

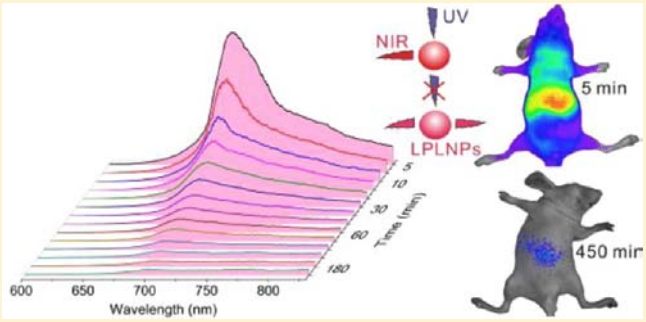


## INTRODUCTION

Optical imaging has received great attention in recent years because of its merits of high sensitivity, cost, and time effectiveness, portability, no harmful radiation, and feasibility for clinical translation, especially its great potential for high-resolution analysis of molecular information on biological tissues and change of physiologic parameters.[1] To date, various luminescent nanoprobes, such as dye-doped nanoparticles,[2] semiconductor quantum dots (QDs),[3] metal nanoclusters,[4] and upconversion nanocrystals,[5] have been applied to optical imaging. However, the necessity for *in situ* excitation of conventional fluorescent probes during *in vivo* imaging produces strong tissue autofluorescence, light scattering and phototoxicity. Recently, several types of nanoprobes such as $Ag_2S$ QDs[6] and carbon nanotubes[7] with tunable emission in the second near-infrared window have been reported for *in vivo* imaging to eliminate the background noise,[8] but *in situ* excitation is still needed during imaging.

The long-lasting afterglow nature of persistent luminescent nanoparticles (PLNPs)[9a] allows optical excitation before bioimaging, and permits detection and imaging without external illumination, thereby avoiding the background noise from *in situ* excitation.[10] Moreover, PLNPs with NIR emission have great advantages for *in vivo* whole body imaging with high signal-to-noise ratio (SNR), deep penetration, and no need for *in situ* excitation. Although the bulky size of persistent phosphors have been rapidly developed in the past decade,[11] the nanoscale counterparts, especially NIR-emitting PLNPs, are still lacking.

In view of their remarkable optical advantages, PLNPs have been applied for therapy, bioimaging, and bioanalysis.[10,12] Chen and Zhang[10a] pioneered the application of PLNPs with attached photosensitizers as an *in vivo* agent for photodynamic therapy. Scherman and co-workers published a milestone paper on *in vivo* bioimaging with NIR-emitting PLNPs ($Ca_{0.2}Zn_{0.9}Mg_{0.9}Si_2O_6:Eu^{2+},Mn^{2+},Dy^{3+}$).[10b] Such PLNPs allowed real-time monitoring of living mice for over 1 h after intravenous injection without external illumination source, and permitted nontargeted imaging of tumor after PEGylation[10b] and *in vitro* targeted imaging of glioma cells[12b] and prostate cancer cells[12c] after further functionalization. Recently, the same group reported two new PLNPs ($CaMgSi_2O_6:Eu^{2+},Mn^{2+},Pr^{3+}$ and $Ca_2Si_5N_8:Eu^{2+},Tm^{3+}$) with improved optical characteristics.[12d,e] Encouraged by the pioneering works in biomedical application of PLNPs,[10] functional green-emitting PLNPs ($Ca_{1.86}Mg_{0.14}ZnSi_2O_7:Eu^{2+},Dy^{3+}$) were also fabricated for detecting $\alpha$-fetoprotein excreted during cancer

Received: April 29, 2013
Published: August 29, 2013

   dx.doi.org/10.1021/ja404243v | J. Am. Chem. Soc. 2013, 135, 14125–14133

cell growth,[12f] while blue-emitting PLNPs ($SrMgSi_2O_6$:$Eu^{2+}$,$Dy^{3+}$) were prepared with mesoporous silica nanospheres as a template for luminescence imaging of a mouse over 1 h after peritoneal injection.[12g] However, the preparation of all the aforementioned PLNPs from $Eu^{2+}$-doped silicate hosts necessitates high-temperature calcination in reducing atmosphere to reduce $Eu^{3+}$ to $Eu^{2+}$, while their afterglow time is still not long enough for long-term *in vivo* imaging. Therefore, there is an urgent need for functional NIR-emitting PLNPs with bright luminescence and long afterglow for long-term targeted tumor imaging *in vivo*.

Recently, $Cr^{3+}$-doped gallate persistent phosphors with NIR emission and long afterglow, such as $ZnGa_2O_4$:$Cr^{3+}$, Ge/Sn substituted $ZnGa_2O_4$:$Cr^{3+}$, and $Zn_3Ga_2Ge_2O_{10}$:$Cr^{3+}$ (360 h afterglow time for ceramic disc), were prepared by a solid-state method without the need for a reducing atmosphere.[13−15] However, these bulky materials are unsuitable for *in vivo* bioimaging. More recently, a novel $Cr^{3+}$-doped $LiGa_5O_8$ NIR phosphor with a persistent luminescence of more than 1000 h in powder form was reported, and *in vivo* imaging could be monitored for more than 4 h in mouse after subcutaneous injection without an illumination source.[12h] In light of the long afterglow time and reducing atmosphere-free preparation, the development of functional $Cr^{3+}$-doped gallogermanate based PLNPs would be promising for targeted bioimaging.

Herein, we report the fabrication, by a citrate sol−gel method in combination with a subsequent reducing atmosphere-free calcination, of functional NIR-emitting long-persistent luminescent nanoparticles (LPLNPs) with a nominal composition[9b] of $Zn_{2.94}Ga_{1.96}Ge_2O_{10}$:$Cr^{3+}$,$Pr^{3+}$. The persistent luminescence intensity and afterglow time of the LPLNPs are significantly improved via codoping $Pr^{3+}/Cr^{3+}$ and creating suitable Zn deficiency in zinc gallogermanate (ZGGO) host. The prepared LPLNPs give distinguished advantages of bright NIR emission, long afterglow time (>15 days for the powder), excellent biocompatibility, and low toxicity, and are promising for long-term *in vivo* bioimaging application.

## RESULTS AND DISCUSSION

**Synthesis and Characterization.** The NIR-emitting LPLNPs were successfully synthesized by a citrate sol−gel method in combination with a subsequent reducing atmosphere-free calcination (see Experimental Section for details). The persistent luminescence intensity and afterglow time of the LPLNPs depended on the pH of the starting solution and calcination temperature. The optimal pH of the starting solution is about 5 (Figure S1 in the Supporting Information (SI)). Calcination temperature no more than 600 °C gave no NIR emission (SI, Figure S2). Increase of calcination temperature led to an increase of the NIR emission at 695 nm in conjunction with a decrease of the host emission. The host emission disappeared at the calcination temperatures higher than 1000 °C (SI, Figure S2). The NIR persistent luminescence intensity increased with increasing of calcination time (SI, Figure S3), probably due to more vacancies of $Ge^{4+}$, $Zn^{2+}$, and oxygen created during calcination.[13,15]

The persistent luminescence intensity and afterglow time of LPLNPs was improved by codoping $Pr^{3+}/Cr^{3+}$ and creating suitable Zn deficiency in ZGGO. The luminescence decay curves of $Zn_3Ga_{2-x-y}Ge_2O_{10}$:$Cr_xPr_y$ varied with the content of doped Pr and Cr (Figure 1a). The persistent luminescence intensity decreased as the content of $Cr^{3+}$ increased because the increased $Cr^{3+}$ emitter in the ZGGO host made a quicker

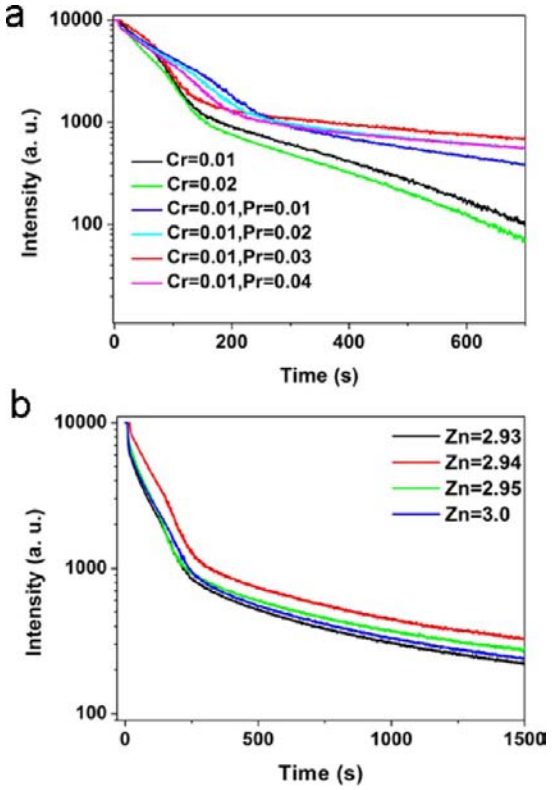


**Figure 1.** The afterglow decay curves of LPLNPs powder after 5 min irradiation with a 254 nm UV lamp: (a) $Zn_3Ga_{2-x-y}Ge_2O_{10}$:$Cr_xPr_y$ with various contents of $Pr^{3+}/Cr^{3+}$. (b) $Zn_zGa_{1.96}Ge_2O_{10}$:$Cr_{0.01}Pr_{0.03}$ with various contents of Zn. Persistent luminescence intensity (logarithmic scale) was monitored at 695 nm as a function of time.

release of the energy of excitation storage and faster decay of persistent emission.[13,15] The $Pr^{3+}/Cr^{3+}$ codoped ZGGO gave more intense persistent luminescence than the single $Cr^{3+}$-doped ZGGO. The most intense persistent luminescence was obtained for $Zn_3Ga_{1.96}Ge_2O_{10}$:$Cr_{0.01}Pr_{0.03}$. The role of $Pr^{3+}$ was probably to prolong the afterglow time through adjusting the trap density and depth because the trivalent lanthanide ions with abundant energy levels of 4f electron configurations can provide more efficient traps to improve the intensity and time of persistent luminescence.[12d,16] Similar results were also observed by other scientists for $CaMgSi_2O_6$:$Eu^{2+}$,$Mn^{2+}$,$Pr^{3+}$ via controlling the electron trap depth with $Pr^{3+}$, and $Sr_2SnO_4$:$Sm^{3+}$,$Dy^{3+}$ via increasing appropriate traps with $Dy^{3+}$.[12d,17]

The control of zinc content not only creates a suitable $Zn^{2+}$ deficiency in LPLNPs to enhance the persistent luminescence intensity, but also facilitates the persistent energy transfer between host emission and $Cr^{3+}$ (SI, Figure S4). Figure 1b shows the NIR luminescence decay curves of $Zn_zGa_{1.96}Ge_2O_{10}$:$Cr_{0.01}Pr_{0.03}$ with various contents of Zn. The persistent luminescence intensity increased as the content of Zn (z) decreased from 3.0 to 2.94 but decreased with a further decrease of z to 2.93. It was reported that a suitable cation deficiency such as the $Zn^{2+}$ deficiency in $ZnGa_2O_4$:$Cr^{3+}$ and $Sr^{2+}$ deficiency in $SrAl_2O_4$:$Eu^{2+}$,$Na^+$ produced more cation vacancies as hole traps to enhance the persistent luminescence intensity.[13,16b]

The X-ray diffraction (XRD) pattern of the LPLNPs is similar to the spinel phase of $ZnGa_2O_4$ (JCPDS file number 38-1240) and $Zn_2GeO_4$ (JCPDS file number 25-1018) (Figure


dx.doi.org/10.1021/ja404243v | J. Am. Chem. Soc. 2013, 135, 14125−14133

2a). No peaks from other phases such as ZnO, $GeO_2$, or $Ga_2O_3$ appear. The actual composition of the LPLNPs was determined

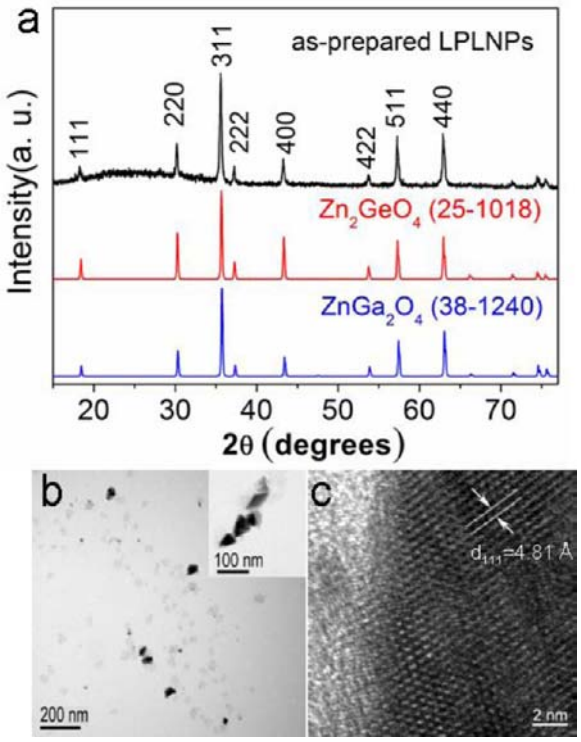


**Figure 2.** (a) XRD patterns of the LPLNPs powder; (b) TEM and (c) high-resolution TEM images of the LPLNPs.

to be $Zn_{2.78}Ga_{1.68}Ge_{1.00}O_8$:$Cr_{0.01}$,$Pr_{0.02}$ by X-ray fluorescence spectrometry. The above results indicate the formation of a pure spinel phase zinc gallogermanate solid solution. Transmission electron microscopy (TEM) reveals nanosized LPLNPs (48.7 ± 15.3 nm, calculated from 100 randomly selected particles) (Figure 2b and SI, Figure S5) and some nonspherical shape with different aspect ratios. Dynamic light scattering analysis shows a hydrodynamic diameter of 71.3 nm with a polydispersity index of 0.253 (SI, Figure S6). The high-resolution TEM analysis indicates that the distance between the lattice fringes is 4.81 Å (Figure 2c), which corresponds to the *d*-spacing for the (111) lattice planes of the spinel zinc gallogermanate. A number of lattice defects were also observed in the high-resolution TEM image of the LPLNPs.

To improve the biocompatibility, solubility, colloidal stability, and blood circulation time,[18] the LPLNPs were PEGylated by coating 3-amino propyltriethoxysilane (APTES) via a condensation reaction of the silanol groups of APTES with surface hydroxyl groups of LPLNPs, and subsequent covalent linking of succinimidyl carbonate-poly (ethylene glycol)-carboxymethyl (SC-PEG-COOH, MW = 3400) to the amino-groups (Figure 3a). Further conjugation of the PEG-LPLNPs with a RGD peptide c(RGDyK) was carried out for tumor-targeted imaging application. The LPLNPs surface modifications with APTES, PEG, and RGD were confirmed by Fourier transform infrared (FT-IR) spectrometry (Figure 3b), Zeta potential (SI, Figure S7), and thermogravimetric analysis (TGA) (Figure 3c). In the FT-IR spectra of APTES-LPLNPs, there are strong absorption bands at 1120 and 1033 $cm^{-1}$ (stretching vibrations of O−Si−O),[19] the asymmetric and symmetric $CH_2$− stretching bands at 2926 and 2855 $cm^{-1}$, and the N−H stretching bands at 3415

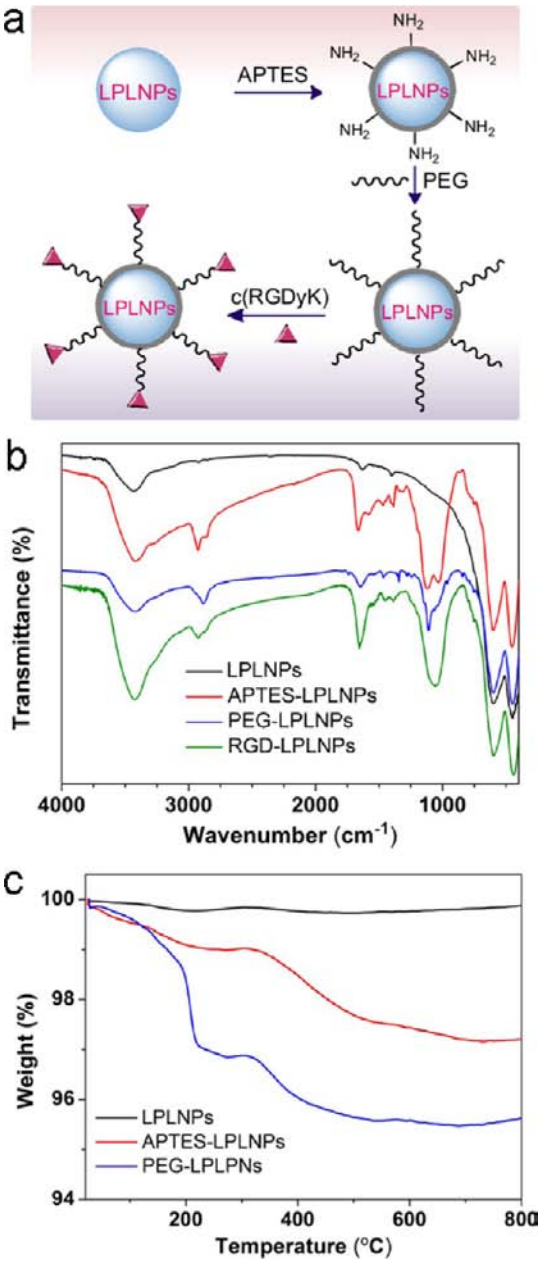


**Figure 3.** (a) Schematic illustration for the surface modification of the LPLNPs; (b) FT-IR spectra of unmodified LPLNPs, APTES-LPLNPs, PEG-LPLNPs, and RGD-LPLNPs; (c) TGA curves of unmodified LPLNPs, APTES-LPLNPs, and PEG-LPLNPs.

and 3284 $cm^{-1}$, indicating the successful modification of LPLNPs with APTES. The FT-IR spectra of PEG-LPLNPs show two absorption bands at 1110 and 2886 $cm^{-1}$ (the C−O bond and the $CH_2$− stretching vibration of PEG chains, respectively), and the absorption band at 1741 $cm^{-1}$ (stretching vibration of C═O), showing the successful PEGylation of the LPLNPs. The appearance of the amide II band at 1541 $cm^{-1}$ in the FT-IR spectra of the RGD-LPLNPs indicates the immobilization of c(RGDyK) peptides on the LPLNPs surface (Figure 3b vs SI, Figure S8).

The bare LPLNPs exhibited negative surface potential at neutral pH (ζ, −27 mV) due to the existence of hydroxyl groups on the surface of the LPLNPs after partial erosion with NaOH solution (SI, Figure S7). In contrast, the APTES-LPLNPs gave positive surface potential (ζ, +13 mV) as a result


dx.doi.org/10.1021/ja404243v | J. Am. Chem. Soc. 2013, 135, 14125−14133

of the protonation of the amino groups at the surface. After PEGylation, the mean hydrodynamic diameter increased to 128.2 nm (SI, Figure S6) while the zeta potential became negative ($\zeta$, −38 mV) (SI, Figure S7) due to the presence of chain-end carboxyl groups on the surface of LPLNPs. Further conjugation with the c(RGDyK) resulted in a slight increase of the mean hydrodynamic diameter to 132.3 nm (SI, Figure S6), but a decrease of the zeta potential to −29 mV (SI, Figure S7).

The amounts of APTES and PEG on the surface of the LPLNPs were estimated by TGA (Figure 3c). A slight weight loss below 125 °C was observed for APTES and PEG-LPLNPs due to the loss of absorbed water. A sharp drop of weight for PEG-LPLNPs occurred in the temperature range of 180−220 °C and well matched the weight loss curve of pure PEG (SI, Figure S9), indicating the pyrolysis of PEG. The weight percentages of organic moieties on APTES-LPLNPs and PEG-LPLNPs were estimated to be 1.9% and 3.9%, respectively. The average number of PEG per LPLNP was evaluated to be 1300 approximately.[10b]

**Persistent Luminescence Properties of the LPLNPs.** Figure 4 shows the excitation and emission spectra of the LPLNPs powder, undoped ZGGO powder, and aqueous dispersion of the LPLNPs at room temperature. Excitation of the LPLNPs powder at 254 nm gave a NIR emission band at 695 nm (Figure 4a) due to the $^2E \rightarrow {}^4A_2$ transition in distorted $Cr^{3+}$ ions in gallogermanate.[13] The excitation spectra of the LPLNPs powder have four main bands with the position and shape (Figure 4a) differing from those of previous reported $Zn_3Ga_2Ge_2O_{10}:Cr^{3+}$.[15] The strong excitation peak at 260 nm probably resulted from the combination of the ZGGO host excitation band and the O−Cr charge transfer band.[20] The other three bands at 407 nm ($^4A_2 \rightarrow {}^4T_1$ ($te^2$) transition), 464 nm ($^4A_2 \rightarrow {}^4T_1$ ($t^2e$) transition), and 558 nm ($^4A_2 \rightarrow {}^4T_2$ transition) originated from the 3d intrashell transitions of $Cr^{3+}$.[15] The self-activated luminescent ZGGO host exhibits a broad white emission band in the range of 350−660 nm with a maximum emission at 505 nm under 254 nm excitation (Figure 4b) likely due to the electrons-holes recombination between the native defects (oxygen-defect, interstitial monovalent Zn, Ge-related centers, Zn-defect, and gallium−oxygen vacancy pair).[21] In contrast, the host emission disappeared after codoping $Cr^{3+}/Pr^{3+}$ into ZGGO due to an effective non-radiative energy transfer between the host emission and the absorption of $Cr^{3+}$ ($^4A_2 \rightarrow {}^4T_1$ ($te^2$), $^4A_2 \rightarrow {}^4T_1$ ($t^2e$) and $^4A_2 \rightarrow {}^4T_2$ transition) resulting from their large spectral overlap (Figure 4b). The result is similar to the energy transfer between the blue emission of $ZnGa_2O_4$ host and the absorption of $Cr^{3+}$.[20] A calcination temperature of 600 °C gave three excitation bands of $Cr^{3+}$, but no excitation peak of LPLNPs powder at 254 nm when the emission wavelength was set at 695 nm (SI, Figure S10). As a result, no NIR emission was observed at a calcination temperature of 600 °C under 254 nm excitation (SI, Figure S2). Instead, a host emission peak at 530 nm was obtained at a calcination temperature of 600 °C under 254 nm excitation due to no energy transfer from the host to $Cr^{3+}$. In contrast, an increase of the calcination temperature to 1000 °C resulted in an intensive NIR emission under 254 nm excitation, but the disappearance of the host emission peak at 530 nm (SI, Figure S2). These observations further confirm the occurrence of the energy transfer from the host to $Cr^{3+}$ in the LPLNPs prepared under the calcination temperature of 1000 °C.

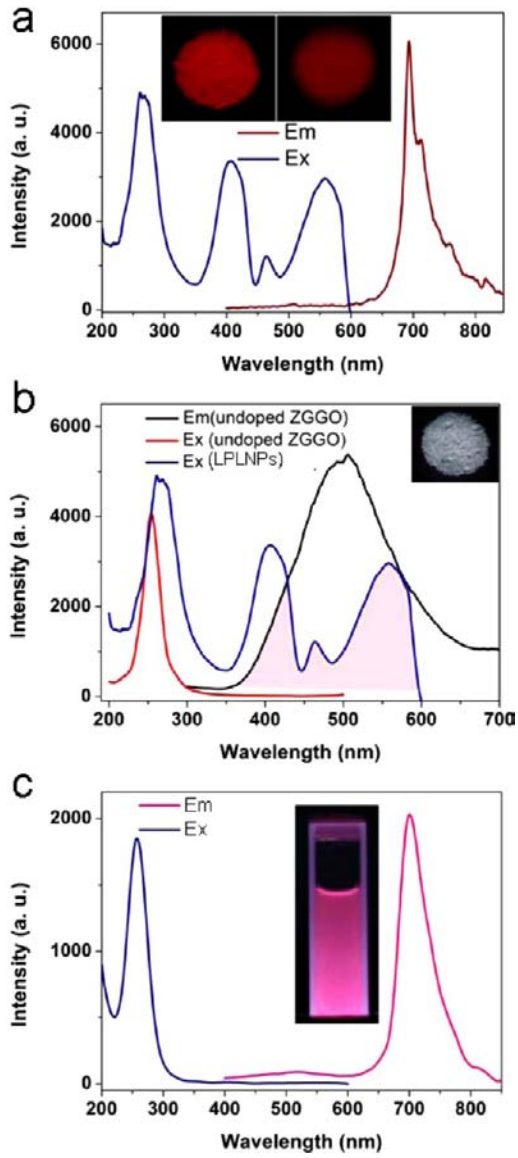


**Figure 4.** (a) Excitation (blue curve, at the emission of 695 nm) and emission (red curve, excitation at 254 nm) spectra of the LPLNPs powder. The inset shows the digital photos of LPLNPs powder under 254 nm UV excitation (left), and 5 s after stopping UV irradiation (right). (b) Excitation spectra of undoped ZGGO powder (red curve) and LPLNPs powder (blue curve) at the emission of 695 nm, and emission spectra of undoped ZGGO powder (black curve) under the excitation of 254 nm. The inset shows the digital photo of undoped ZGGO powder under 254 nm UV excitation. (c) Excitation (blue curve, emission at 700 nm) and emission (red curve, excitation at 254 nm) spectra of the aqueous dispersion of LPLNPs (1 mg $mL^{-1}$). The inset shows the digital photo of the aqueous dispersion of LPLNPs under 254 nm UV excitation.

For the LPLNPs colloidal solution, a strong emission band at 700 nm and a much weaker band at 521 nm were observed under 254 nm excitation (Figure 4c), indicating that the energy transfer was still effective in water. Compared to the LPLNPs powder, only host excitation peak remained while other excitation bands disappeared in the LPLNPs colloidal solution probably due to the quenching effect of the O−H vibration of water.[22] Moreover, the aqueous colloidal solution of LPLNPs gave much shorter photoluminescence lifetime (2.86 ± 0.05 s) than the LPLNPs powder (47.55 ± 1.65 s) (SI, Figure S11 and


dx.doi.org/10.1021/ja404243v | J. Am. Chem. Soc. 2013, 135, 14125−14133

S12; Table S1). The absolute photoluminescence quantum yield of the aqueous dispersion of LPLNPs is 1.3%, comparable to those of NIR emitting $Ag_2Se$,[23a] $Ag_2X$ (X: S, Se, Te) QDs,[23b] and carbon nanotubes,[7a] but lower than those of recently improved $Ag_2S$ and $Ag_2Se$ QDs.[23c,d]

The as-synthesized LPLNPs exhibit excellent long-lasting NIR luminescence. The NIR emission decays of the LPLNPs powder after 5 min irradiation with a 254 nm UV lamp (6 W) are shown in Figure 5. The persistent luminescence decayed

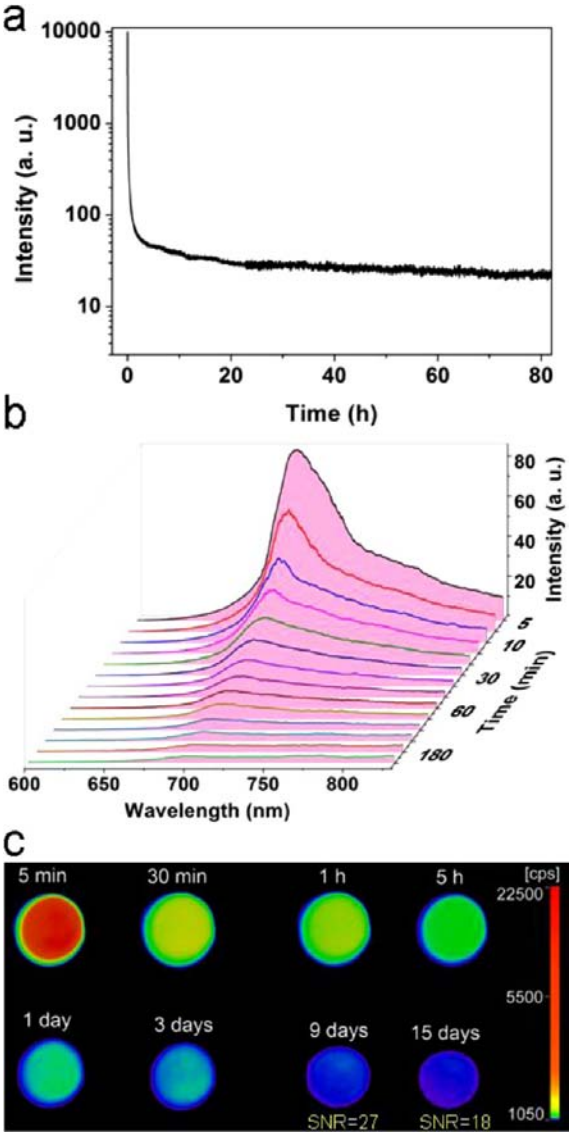


**Figure 5.** NIR afterglow decay of LPLNPs powder after 5 min irradiation with a 254 nm UV lamp: (a) persistent luminescence intensity monitored at 695 nm as a function of time (logarithmic scale); (b) time-dependent persistent luminescence spectra; (c) NIR afterglow decay images recorded by CCD camera at different times after stopping UV irradiation.

fast at the beginning, and then slowly (Figure 5a,b). The deep red persistent luminescence could be discerned by naked eyes and captured using a digital camera 5 s after stopping UV excitation (inset in Figure 4a). The NIR persistent luminescence was still detectible with a SNR of 18 by a CCD camera for 15 days without any external illumination (Figure 5c; SI, Figure S13). The afterglow time of the LPLNPs powder was thus estimated to be more than 15 days, similar to that for a $Zn_3Ga_2Ge_2O_{10}:Cr^{3+}$ ceramic disc.[15]

The LPLNPs colloids still show a bright NIR persistent luminescence. Figure 6a shows the NIR emission decay curve

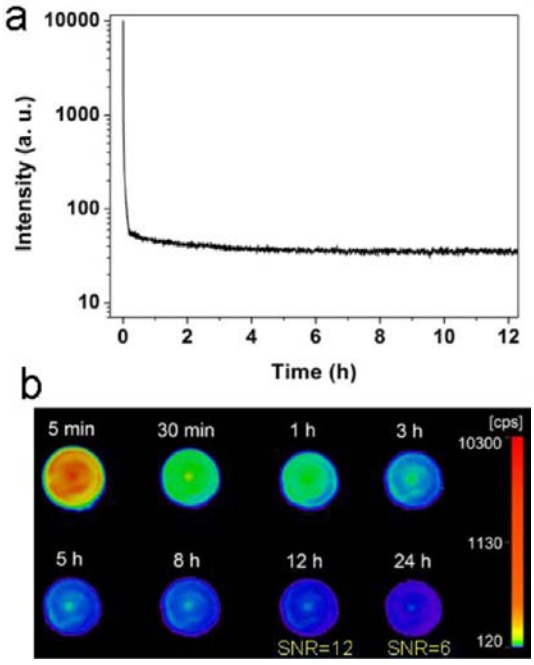


**Figure 6.** NIR afterglow decay of aqueous dispersion of the LPLNPs (1 mg $mL^{-1}$) after 5 min of irradiation with a 254 nm UV lamp: (a) Persistent luminescence intensity monitored at 700 nm (logarithmic scale) as a function of time. (b) NIR afterglow decay images obtained by a CCD camera at different times after stopping UV irradiation.

of the aqueous LPLNPs colloids (1 mg $mL^{-1}$) monitored at 700 nm after 5 min of UV irradiation. The NIR luminescence of the LPLNPs colloidal solution (1 mg $mL^{-1}$) was also detectable with a SNR of 6 by a CCD camera even 24 h after stopping UV excitation (Figure 6b; SI, Figure S14). The colloidal solution of the LPLNPs shows a shorter afterglow time than the LPLNPs powder because of the low density of the LPLNPs in water. The superlong NIR persistent luminescence properties of LPLNPs guarantee long-term *in vivo* imaging with high SNR.

The persistent energy transfer mechanism between ZGGO host and $Cr^{3+}$ ion is illustrated in Figure 7. Upon 254 nm UV excitation, the incident photons are absorbed by ZGGO host and the electrons are promoted from the valence band of ZGGO to the conduction band. Subsequently, the excited free electrons are captured by native defects via nonradiative relaxation. After UV irradiation is stopped, the recombination of electrons and holes released from native defects results in a broadband persistent luminescence (Figure 4b and SI, Figure S15). Because of sufficient spectral overlap between the host emission and the three absorption bands of $Cr^{3+}$ (Figure 4b), the energy of the host is persistently transferred to the $Cr^{3+}$ ion slowly via an effective nonradiative energy transfer.[24] The persistent energy transfer leads to the simultaneous promotion of the 3d electrons of $Cr^{3+}$ from ground-state ($^4A_2$) to three different energy levels of excited-states ($^4T_1$ ($te^2$), $^4T_1$ ($t^2e$) and $^4T_2$). The excited electrons at the excited-state of $^4T_1$ ($te^2$) are captured by shallow electron traps through a conduction band and can be transferred to deep traps via nonradiative


dx.doi.org/10.1021/ja404243v | J. Am. Chem. Soc. 2013, 135, 14125−14133

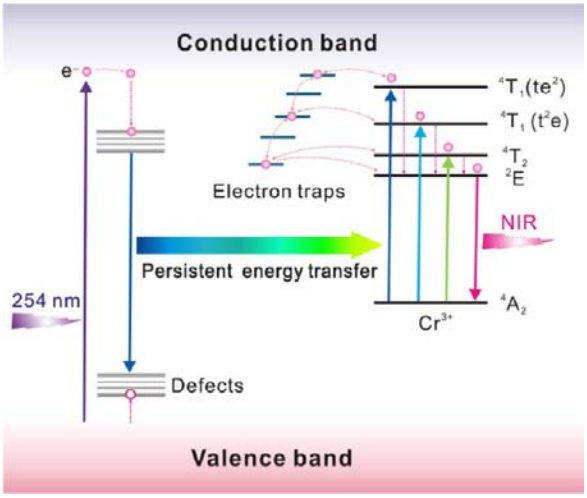


**Figure 7.** Schematic illustration of the persistent energy transfer mechanism between ZGGO host and $Cr^{3+}$ ion. Dotted-line arrows represent nonradiative electron (or hole) transfer processes.

relaxation.[15] Meanwhile, the energy matched traps are filled with electrons at levels of $^4T_1$ ($t^2e$) and $^4T_2$ via a tunneling process.[25] After the persistent energy transfer stops, the electrons released from shallow traps are directly recombined with ionized $Cr^{3+}$ and produce a strong persistent luminescence at the beginning. The slow reverse tunneling recombination for other electrons released from deeper traps occurs a while later and probably causes superlong persistent luminescence.

**Toxicity, Bidistribution, and *in Vivo* NIR Luminescence Imaging.** The cytotoxicity of the LPLNPs was tested on 3T3 normal cell lines and U87MG cancer cell lines by cell counting assay (see the SI). The viability of two type cells was still greater than 80% after incubation of the cell lines with the PEG-LPLNPs even with the concentration as high as 1000 $\mu$g $mL^{-1}$ for 24 h (SI, Figure S16a). The *in vivo* toxicity of PEG-LPLNPs was also evaluated via monitoring histological changes in several susceptible organs including heart, liver, spleen, lung, and kidney to show whether PEG-LPLNPs could cause any harmful effect during retention in the mouse body for 7 days (see the SI). The results show that no significant evidence for organ damage or inflammatory lesion associated with the administration of PEG-LPLNPs was detected (SI, Figure S16b). Furthermore, the long-term toxic effect of PEG-LPLNPs was assessed using mice (SI, Figure S16c). After 30 days of PEG-LPLNPs injection, the mice viability was still 100%, and there was no significant difference between the body weights of control and treated mice. The above results indicate the low toxicity of the PEG-LPLNPs.

The persistent luminescence properties of LPLNPs were also tested in living animal tissue. PEG-LPLNPs solution (1 mg $mL^{-1}$) in phosphate buffered saline (PBS) was excited for 10 min using a 254 nm UV lamp before injection. The pre-excited PEG-LPLNPs solution (0.4 mL) was administrated into a normal mouse through subcutaneous injection to make a direct comparison with the $Cr^{3+}$-doped $LiGa_5O_8$ phosphor.[12h] The results show that the PEG-LPLNPs gave a very high SNR of 1826 at 5 min postinjection, and allow *in vivo* bioimaging to be monitored (SNR > 5) for more than 15 h in mouse after subcutaneous injection without an illumination source (Figure 8a), much longer than 4 h for the $Cr^{3+}$-doped $LiGa_5O_8$.[12h] To evaluate the stimulation ability of the LPLNPs by a NIR light,

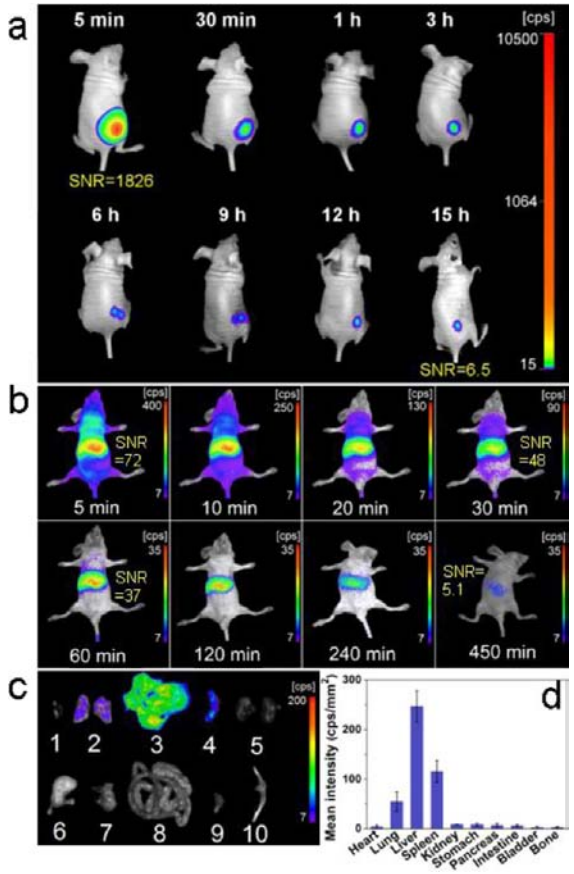


**Figure 8.** (a) *In vivo* NIR luminescence images of a normal mouse after subcutaneous injection of PEG-LPLNPs (0.4 mg, 10 min irradiation with a 254 nm UV lamp before injection). (b) *In vivo* NIR luminescence images of a normal mouse after intravenous injection of PEG-LPLNPs (0.6 mg, 10 min irradiation with a 254 nm UV lamp before injection). (c) Representative *ex vivo* NIR luminescence images of isolated organs from a normal mouse at 24 h postintravenous injection of PEG-LPLNPs (0.4 mg): (1) heart, (2) lung, (3) liver, (4) spleen, (5) kidney, (6) stomach, (7) pancreas, (8) intestine, (9) bladder, (10) bone. (d) Semiquantification of PEG-LPLNPs in the isolated organs of mice, error bars represent one standard deviation of triplicate measurements from individual animals.

the whole-body mouse was illuminated by a continuous-wave 980 nm laser (the power density of ~40 mW $cm^{-2}$) for 10 s after the persistent luminescence signal totally disappeared (at 5 days postinjection). The persistent luminescence signal was repeatedly recovered after the stimulation (SI, Figure S17), and a detectable luminescence signal was observed even 11 days after the injection, demonstrating that the LPLNPs has a potential application for long-term *in vivo* imaging via repeated stimulation with a NIR light. Furthermore, the pre-excited PEG-LPLNPs solution (0.6 mL) was injected into a normal mouse through the tail vein. *In vivo* luminescence images were collected for more than 450 min without any excitation source (Figure 8b). The reticulo-endothelial system (RES) organs of the mouse were clearly visualized in the presence of the LPLNPs, and the persistent luminescence with a SNR of 72 was obtained in the liver site at the beginning. Although the persistent luminescence intensity of the LPLNPs gradually decreased, the persistent luminescence with a SNR of 5.1 was still observed at 450 min (7.5 h) after injection (SI, Figure S18). The results show that our LPLNPs allow *in vivo*


dx.doi.org/10.1021/ja404243v | J. Am. Chem. Soc. 2013, 135, 14125−14133

bioimaging to be monitored for a much longer time even after intravenous injection in comparison to the $Cr^{3+}$-doped $LiGa_5O_8$ NIR phosphor after subcutaneous injection without *in situ* excitation,[12h] demonstrating the advantages of our LPLNPs for long-term *in vivo* bioimaging without the need for *in situ* excitation.

The relative long-term biodistribution of the LPLNPs in normal mice was evaluated through *ex vivo* NIR luminescence imaging of harvested organs at 24 h postintravenous injection of PEG-LPLNPs (0.4 mg) (see the SI). As shown in Figure 8c, almost no luminescence signals were observed in the heart and bladder while the highest intensive luminescence was observed in the liver. These results are very consistent with the whole-body *in vivo* imaging (Figure 8b) because the LPLNPs not only can avoid the background noise from *in situ* excitation, but also can emit a bright NIR light in the bioimaging window. The luminescence intensity of *ex vivo* imaging is close to a true reflection of the LPLNPs-retained inside the organs in *ex vivo* images. The region-of-interest function analysis on the *ex vivo* luminescence images was performed to semiquantitatively study the biodistribution of PEG-LPLNPs in each individual organs using the indiGO software (Figure 8d). The results indicate that the PEG-LPLNPs were mainly accumulated in liver and spleen, similar to several other materials with similar particle size, such as PEG-grafted PLNP,[12a] luminescent porous silicon nanoparticles,[26a] and gold nanoshells,[26b] because nanoparticles with a lager hydrodynamic size (>100 nm) are mainly uptaken by RES organs.[26c,d] Therefore, it is necessary to develop a general approach for the fabrication of ultrasmall uniform LPLNPs for *in vivo* bioimaging in the near future.

To evaluate the targeting capability of the RGD function-alized-LPLNPs (RGD-LPLNPs), the *in vitro* cell imaging was performed on U87MG cells incubated with PEG-LPLNPs and RGD-LPLNPs (SI, Figure S19). RGD-LPLNPs treated cells gave a much stronger and denser luminescence signal than PEG-LPLNPs treated cells, showing the good targeting capability of RGD-LPLNPs because of the high specific interaction between RGD and integrin $\alpha_v\beta_3$ on the U87MG cells.[27]

To investigate the potential of RGD-LPLNPs for *in vivo* tumor imaging, PEG-LPLNPs and RGD-LPLNPs were respectively injected via tail vein (0.4 mg per mouse) into U87MG tumor-bearing mice and normal mice for comparison. Figure 9 shows that both PEG-LPLNPs and RGD-LPLNPs were rapidly circulated all over animal body within 9 min, and noticeable luminescence signals were observed in tumor sites (Figure 9a,b), indicating the accumulation of the LPLNPs in the tumor site. Although persistent luminescence intensity of the LPLNPs gradually decreased with time without *in situ* excitation, the luminescence signals still appeared in tumor sites at 12 min postintravenous injection. In contrast, almost no luminescence signals were observed in the lower abdominal regions of normal mice (Figure 9c,d). After 20 min post-injection, the luminescence signal of PEG-LPLNPs almost disappeared from tumor sites, whereas the luminescence signal from RGD-LPLNPs was still observed in the tumor site. These facts show that the concentration of the RGD-LPLNPs is higher than that of the PEG-LPLNPs in the tumor site, due to the high affinity of the RGD-LPLNPs to integrin $\alpha_v\beta_3$ on tumor vasculature.[27] Furthermore, a noticeable luminescence signal observed from the *ex vivo* luminescence image of a tumor (Figure 9e,f) also indicates a specific targeting of RGD-LPLNPs for U87MG tumor.

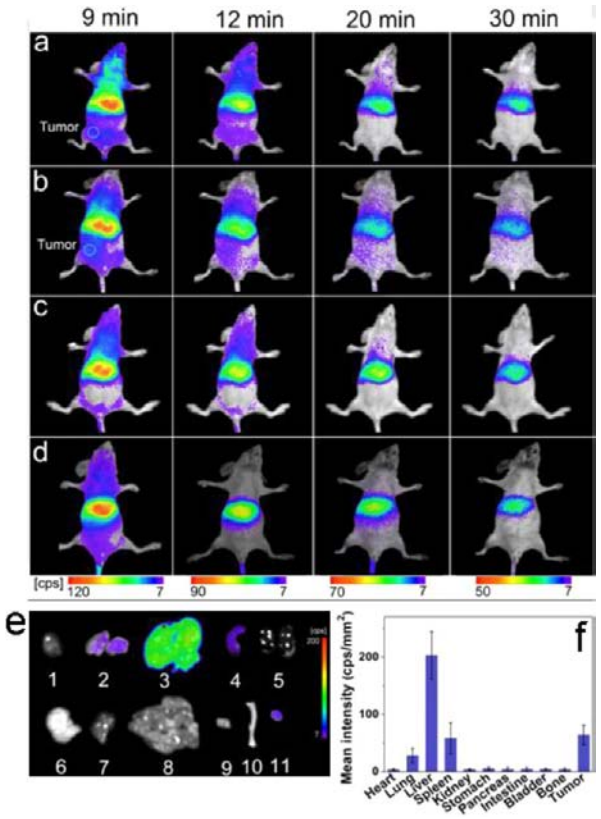


**Figure 9.** *In vivo* NIR luminescence images of U87MG tumor-bearing mice (white circles locate the tumor site): (a,b) and normal mice, (c,d) after intravenous injection of PEG-LPLNPs (a, c) and RGD-LPLNPs (b, d) (0.4 mg, 10 min irradiation with a 254 nm UV lamp before injection). (e) Representative *ex vivo* NIR luminescence images of isolated organs and tumor from a U87MG tumor-bearing mouse at 6 h postintravenous injection of RGD-LPLNPs (0.4 mg): (1) heart, (2) lung, (3) liver, (4) spleen, (5) kidney, (6) stomach, (7) pancreas, (8) intestine, (9) bladder, (10) bone, (11) tumor. (f) Semiquantification of RGD-LPLNPs in the isolated organs and tumor of the mice, error bars represent one standard deviation of triplicate measurements from individual animals.

## ■ CONCLUSIONS

We have demonstrated the synthesis and characterization of functional $Pr^{3+}/Cr^{3+}$ codoped NIR luminescent LPLNPs with superlong lasting afterglow (>360 h) for *in vivo* bioimaging. The co-doping of $Pr^{3+}/Cr^{3+}$ and control of Zn deficiency significantly improve the persistent luminescence property of the LPLNP. Further PEGylation and bioconjugation make the LPLNPs promising as an ideal optical imaging contrast agent for bioimaging. The observed persistent energy transfer between host and $Cr^{3+}$ ion in LPLNPs may also exist in other $Cr^{3+}$-doped gallate persistent phosphors. The prepared LPLNPs offer long afterglow time, good biocompatibility, low toxicity, and bright NIR emission, and hold great potential for long-term *in vivo* bioimaging application with high SNR without the need for *in situ* excitation.

## ■ EXPERIMENTAL SECTION

**Synthesis of LPLNPs.** The LPLNPs were synthesized by a citrate sol−gel method in combination with a subsequent calcination in air. $Zn(NO_3)_2{\cdot}6H_2O$, $Pr(NO_3)_3{\cdot}6H_2O$, $Cr(NO_3)_3{\cdot}9H_2O$, and citric acid were dissolved in ultrapure water. $Ga_2O_3$ was dissolved in dilute nitric acid solution. $GeO_2$ was dissolved in dilute ammonium hydroxide


dx.doi.org/10.1021/ja404243v | J. Am. Chem. Soc. 2013, 135, 14125−14133

solution. The starting material composition of the LPLNPs was modified from that described in a previous publication,[15] and the aqueous solutions of $Zn^{2+}$, $Pr^{3+}$, $Cr^{3+}$, $Ge^{4+}$, and $Ga^{3+}$ were mixed according to the chemical formula of $Zn_zGa_{2-x-y}Ge_2O_{10}:Cr_x\ Pr_y$ ($x$, 0.01−0.02; $y$, 0−0.04; $z$, 2.93−3.0). To the mixture solution, citric acid solution was slowly added without any precipitation, and the molar ratio of total metal ions to citric acid was maintained at 1:1.5, followed by the addition of ammonia hydroxide to adjust the pH to 5. The final solution was vigorously stirred at room temperature for 2 h, then heated in an oven at 75 °C for the slow evaporation of water until the solution became a sol that finally became a gel. The obtained gel was first dried in an oven at 130 °C for 3 h, and then heated at 200 °C for 7 h to form black porous materials. Finally, the porous materials were ground and annealed in air at 1000 °C for 3 h.

**Surface Functionalization of LPLNPs.** The size selection of LPLNPs and modification with APTES were conducted according to existing protocols with slight modification.[10b] The LPLNP powder was wet ground in minimum ethanol for 30 min. The obtained sample was dispersed in 5 mM NaOH solution by sonication for 1 h, and then vigorously stirred for 24 h. The resulting colloid solution was centrifuged at 4000 rpm for 30 min to remove large size particles, and the supernatant was centrifuged at 9000 rpm for 7 min to collect the precipitate. A 5 mg sample of dry precipitate was redispersed in 2 mL of dimethylformamide (DMF) by sonication, and 20 μL of APTES was added under vigorous stirring at 80 °C for 24 h. The resulting APTES-LPLNPs were collected by centrifugation, and washed with DMF to remove unreacted APTES.

A 5 mg portion of APTES-LPLNPs was dispersed in 0.1 M PBS (pH 7.4) by sonication, and 35 mg of PEG was added. The mixture was gently stirred overnight in the dark at room temperature. The unreacted PEG was removed by centrifugation, and the resulting PEG-LPLNPs were washed three times with 10 mM PBS.

To conjugate RGD to the PEG-LPLNPs, 5 mg of PEG-LPLNPs was dispersed in 10 mM PBS (pH 6), and EDC (4 mg) and NHS (10 mg) were added. The mixture was gently stirred at room temperature for 2 h. Following activation, 18 mg of c(RGDyK) was added, and the mixture solution was adjusted to pH 8 with NaOH solution and stirred in the dark at room temperature for 8 h. The unreacted c(RGDyK) was removed by centrifugation and the resulting RGD-LPLNPs were washed three times with 10 mM PBS.

**Characterization.** XRD patterns were recorded on a D/max-2500 diffractometer (Rigaku, Japan) using Cu K$\alpha$ radiation ($\lambda$ = 1.5418 Å). TEM and high-resolution TEM images were obtained on a JEOL-100CX II microscope and a JEM-2100F field emission transmission electron microscope (JEOL, Japan), respectively. The samples for TEM were obtained by drying sample droplets from a water dispersion onto a 300-mesh Cu grid coated with a carbon film, which was then allowed to dry prior to imaging. The actual composition of LPLNPs was determined on a Magix PW2403 X-ray fluorescence spectrometer (PANalytical, Netherlands). Photoluminescence spectra were recorded on an F-4500 spectrofluorometer (Hitachi, Japan). The photoluminescence quantum yield of LPLNPs was determined on an FLS920 spectrometer with an integration sphere attachment under excitation of 254 nm (Edinburgh, UK). FT-IR spectra (4000−400 $cm^{-1}$) in KBr were recorded on a Magna-560 spectrometer (Nicolet, Madison, WI). The hydrodynamic size and zeta potential (at neutral pH) of LPLNPs were measured on a Zetasizer Nano-ZS with 633 nm He−Ne laser (Malvern, UK). TGA experiments were performed on a TG209 thermal analyzer (Netzsch, Germany) under pure $N_2$ in the range from 20 to 800 °C with a heating rate of 10 °C $min^{-1}$. The microscopic images were observed on an IX81 motorized inverted microscope (Olympus, Japan). NIR afterglow decay images were acquired on a Berthold NightOWL LB 983 Imaging System (Bad Wildbad, Germany) equipped with a cooled CCD camera.

***In Vivo* Luminescence Imaging.** *In vivo* experiments were performed on anesthetized mice with chloral hydrate (200 μL, 4%). PEG-LPLNPs or RGD-LPLNPs (1 mg $mL^{-1}$) dispersed in 10 mM PBS solution were injected through the tail vein into normal nude mice or U87MG tumor-bearing mice. The LPLNPs were excited 10 min with a 254 nm UV lamp (6 W) before injection, and luminescence images were immediately acquired after injection. *In vivo* luminescence images of the mice were acquired on a Berthold NightOWL LB 983 Imaging System without excitation sources. The emission filter was set as 700 nm, and the exposure time was set as 120 s.

## ■ ASSOCIATED CONTENT

### Ⓢ Supporting Information

Materials and reagents, cytotoxicity assay, animal model, *ex vivo* biodistribution analysis, calculation of SNR, additional figures and tables as noted in the text. This material is available free of charge via the Internet at http://pubs.acs.org.

## ■ AUTHOR INFORMATION


### Corresponding Author

xpyan@nankai.edu.cn

### Present Address

[§]A.A.: On leave from the Department of Chemistry and Environmental Sciences, Kashgar Teachers College, Kashgar, 844008, China.


### Notes

The authors declare no competing financial interest.

## ■ ACKNOWLEDGMENTS

This work was supported by the National Basic Research Program of China (Grant 2011CB707703), the National Natural Science Foundation of China (Grants 21275079, 20935001), and the Fundamental Research Funds for the Central Universities.

## ■ REFERENCES


(1) (a) Weissleder, R.; Pittet, M. J. *Nature* **2008**, *452*, 580. (b) Louie, A. *Chem. Rev.* **2010**, *110*, 3146. (c) Hellebust, A.; Richards-Kortum, R. *Nanomedicine* **2012**, *7*, 429.

(2) Yan, J.; Estévez, M. C.; Smith, J. E.; Wang, K.; He, X.; Wang, L.; Tan, W. *Nano Today* **2007**, *2*, 44.

(3) (a) Michalet, X.; Pinaud, F. F.; Bentolila, L. A.; Tsay, J. M.; Doose, S.; Li, J. J.; Sundaresan, G.; Wu, A. M.; Gambhir, S. S.; Weiss, S. *Science* **2005**, *307*, 538. (b) Medintz, I. L.; Uyeda, H. T.; Goldman, E. R.; Mattoussi, H. *Nat. Mater.* **2005**, *4*, 435.

(4) (a) Dreaden, E. C.; Alkilany, A. M.; Huang, X.; Murphy, C. J.; El-Sayed, M. A. *Chem. Soc. Rev.* **2012**, *41*, 2740. (b) Shang, L.; Dong, S.; Nienhaus, G. U. *Nano Today* **2011**, *6*, 401.

(5) (a) Zhou, J.; Liu, Z.; Li, F. *Chem. Soc. Rev.* **2012**, *41*, 1323. (b) Haase, M.; Schafer, H. *Angew. Chem., Int. Ed.* **2011**, *50*, 5808.

(6) Hong, G.; Robinson, J. T.; Zhang, Y.; Diao, S.; Antaris, A. L.; Wang, Q.; Dai, H. *Angew. Chem., Int. Ed.* **2012**, *51*, 9818.

(7) (a) Welsher, K.; Liu, Z.; Sherlock, S. P.; Robinson, J. T.; Chen, Z.; Daranciang, D.; Dai, H. *Nat. Nanotechnol.* **2009**, *4*, 773. (b) Robinson, J. T.; Hong, G.; Liang, Y.; Zhang, B.; Yaghi, O. K.; Dai, H. *J. Am. Chem. Soc.* **2012**, *134*, 10664.

(8) Smith, A. M.; Mancini, M. C.; Nie, S. *Nat. Nanotechnol.* **2009**, *4*, 710.

(9) (a) Afterglow emission means the emission after removing exciting source, also called persistent luminescence. (b) Nominal composition refers to the starting material composition, rather than the actual composition of the LPLNPs. For convenience, the composition for the LPLNPs used in the text refers to the nominal composition if no specific description was given.

(10) (a) Chen, W.; Zhang, J. *J. Nanosci. Nanotechnol.* **2006**, *6*, 1159. (b) le Masne de Chermont, Q.; Chaneac, C.; Seguin, J.; Pelle, F.; Maitrejean, S.; Jolivet, J. P.; Gourier, D.; Bessodes, M.; Scherman, D. *Proc. Natl. Acad. Sci. U.S.A.* **2007**, *104*, 9266.

(11) Van den Eeckhout, K.; Smet, P. F.; Poelman, D. *Materials* **2010**, *3*, 2536.

(12) (a) Maldiney, T.; Richard, C.; Seguin, J.; Wattier, N.; Bessodes, M.; Scherman, D. *ACS Nano* **2011**, *5*, 854. (b) Maldiney, T.;

Kaikkonen, M. U.; Seguin, J.; le Masne de Chermont, Q.; Bessodes, M.; Airenne, K. J.; Ylä-Herttuala, S.; Scherman, D.; Richard, C. *Bioconjugate. Chem.* **2012**, *23*, 472. (c) Maldiney, T.; Byk, G.; Wattier, N.; Seguin, J.; Khandadash, R.; Bessodes, M.; Richard, C.; Scherman, D. *Int. J. Pharm.* **2012**, *423*, 102. (d) Maldiney, T.; Lecointre, A. l.; Viana, B.; Bessière, A. l.; Bessodes, M.; Gourier, D.; Richard, C.; Scherman, D. *J. Am. Chem. Soc.* **2011**, *133*, 11810. (e) Maldiney, T.; Kaikkonen, M. U.; Seguin, J.; le Masne de Chermont, Q.; Bessodes, M.; Airenne, K. J.; Yla-Herttuala, S.; Scherman, D.; Richard, C. *Opt. Mater. Express* **2012**, *2*, 261. (f) Wu, B.-Y.; Wang, H.-F.; Chen, J.-T.; Yan, X.-P. *J. Am. Chem. Soc.* **2011**, *133*, 686. (g) Li., Z.-J.; Zhang, H.-W.; Sun, M.; Shen, J.-S.; Fu, H.-X. *J. Mater. Chem.* **2012**, *22*, 24713. (h) Liu, F.; Yan, W.; Chuang, Y.-J.; Zhen, Z.; Xie, J.; Pan, Z. *Sci. Rep.* **2013**, *3*, 1554.

(13) Bessiere, A.; Jacquart, S.; Priolkar, K.; Lecointre, A.; Viana, B.; Gourier, D. *Opt. Express* **2011**, *19*, 10131.

(14) Allix, M.; Chenu, S.; Véron, E.; Poumeyrol, T.; Kouadri-Boudjelthia, E. A.; Alahraché, S.; Porcher, F.; Massiot, D.; Fayon, F. *Chem. Mater.* **2013**, *25*, 1600.

(15) Pan, Z.; Lu, Y.-Y.; Liu, F. *Nat. Mater.* **2012**, *11*, 58.

(16) (a) Jia, D.; Lewis, L. A.; Wang, X.-j. *Electrochem. Solid State* **2010**, *13*, J32. (b) Aitasalo, T.; Dereń, P.; Hölsä, J.; Jungner, H.; Krupa, J. C.; Lastusaari, M.; Legendziewicz, J.; Niittykoski, J.; Stręk, W. *J. Solid State Chem.* **2003**, *171*, 114.

(17) Yu, X.; Xu, X. H.; Qiu, J. B. *Mater. Res. Bull.* **2011**, *46*, 627.

(18) Karakoti, A. S.; Das, S.; Thevuthasan, S.; Seal, S. *Angew. Chem., Int. Ed.* **2011**, *50*, 1980.

(19) Schladt, T. D.; Koll, K.; Prüfer, S.; Bauer, H.; Natalio, F.; Dumele, O.; Raidoo, R.; Weber, S.; Wolfrum, U.; Schreiber, L. M.; Radsak, M. P.; Schild, H.; Tremel, W. J. *Mater. Chem.* **2012**, *22*, 9253.

(20) Kim, J. S.; Kim, J. S.; Park, H. L. *Solid State Commun.* **2004**, *131*, 735.

(21) (a) Liu, Z.; Jing, X.; Wang, L. *J. Electrochem. Soc.* **2007**, *154*, H500. (b) Binet, L.; Gourier, D. *J. Phys. Chem. Solids* **1998**, *59*, 1241. (c) Gao, G.; Wondraczek, L. *J. Mater. Chem. C* **2013**, *1*, 1952. (d) Takahashi, Y.; Ando, M.; Iwasaki, K.; Masai, H.; Fujiwara, T. *Appl. Phys. Lett.* **2010**, *97*, 071906.

(22) Eliseeva, S. V.; Bunzli, J.-C. G. *Chem. Soc. Rev.* **2010**, *39*, 189.

(23) (a) Gu, Y. P.; Cui, R.; Zhang, Z. L.; Xie, Z. X.; Pang, D. W. *J. Am. Chem. Soc.* **2012**, *134*, 79. (b) Yarema, M.; Pichler, S.; Sytnyk, M.; Seyrkammer, R.; Lechner, R. T.; Fritz-Popovski, G.; Jarzab, D.; Szendrei, K.; Resel, R.; Korovyanko, O.; Loi, M. A.; Paris, O.; Hesser, G.; Heiss, W. *ACS Nano* **2011**, *5*, 3758. (c) Zhang, Y.; Hong, G. S.; Zhang, Y. J.; Chen, G. C.; Li, F.; Dai, H. J.; Wang, Q. B. *ACS Nano* **2012**, *6*, 3695. (d) Dong, B. H.; Li, C. Y.; Chen, G. C.; Zhang, Y. J.; Zhang, Y.; Deng, M. J.; Wang, Q. B. *Chem. Mater.* **2013**, *25*, 2503.

(24) Kuang, J.; Liu, Y. *Chem. Phys. Lett.* **2006**, *424*, 58.

(25) (a) Lecointre, A.; Bessière, A.; Bos, A. J. J.; Dorenbos, P.; Viana, B.; Jacquart, S. *J. Phys. Chem. C* **2011**, *115*, 4217. (b) Delbecq, C. J.; Toyozawa, Y.; Yuster, P. H. *Phys. Rev. B* **1974**, *9*, 4497.

(26) (a) Park, J.-H.; Gu, L.; von Maltzahn, G.; Ruoslahti, E.; Bhatia, S. N.; Sailor, M. J. *Nat. Mater.* **2009**, *8*, 331. (b) James, W. D.; Hirsch, L. R.; West, J. L.; O'Neal, P. D.; Payne, J. D. *J. Radioanal. Nucl. Chem.* **2007**, *271*, 455. (c) Jokerst, J. V.; Gambhir, S. S. *Acc. Chem. Res.* **2011**, *44*, 1050. (d) Longmire, M.; Choyke, P. L.; Kobayashi, H. *Nanomedicine* **2008**, *3*, 703.

(27) Schottelius, M.; Laufer, B.; Kessler, H.; Wester, H.-J. r. *Acc. Chem. Res.* **2009**, *42*, 969.